Genomic Analysis of Non-NF2 Meningiomas Reveals Mutations in TRAF7, KLF4, AKT1, and SMO

Victoria E. Clark *et al.*

Science **339**, 1077 (2013);
DOI: 10.1126/science.1233009

Science (print ISSN 0036-8075; online ISSN 1095-9203) is published weekly, except the last week in December, by the American Association for the Advancement of Science, 1200 New York Avenue NW, Washington, DC 20005.

these sequences are recognized as functional enhancers, yet actively repressed.

To test the functionality of STARR-seq enhancers when integrated into the genome, we created 22 stable S2 cell lines each carrying stably integrated luciferase reporter constructs with an enhancer (15 lines) or a negative fragment (fig. S21). All enhancers, including three out of three closed enhancers, showed strong luciferase activity, whereas none of the negative controls did (Fig. 3C and fig. S21). For all, the luciferase activity was constant over a course of 4 weeks, measured 3, 5, and 7 weeks after integration (fig. S21). The activity of the three closed enhancers suggests that their endogenous inactive state might depend on the genomic context and/or on regulatory activities in S2 precursor cells. This shows that enhancers identified by ectopic assays, such as STARR-seq, can function when integrated into a chromosomal context, even if they are silenced endogenously.

We next applied STARR-seq to *Drosophila* adult ovarian somatic cells [OSCs (*21*)] and identified a comparable number of enhancers (4682; $P \leq 0.001$, binomial test; FDR = 0.2%) with similar characteristics (figs. S4B; S5B; S6, C to E; S12D; S13, C and D; and S22, A to C). Out of 8659 enhancers found in S2 cells or OSCs, 5404 (62.4%) changed at least twofold and 2138 (24.7%) at least fourfold between both cell types (Fig. 4A, and figs. S23 and S24, A and D), and luciferase assays confirmed these differences quantitatively ($r = 0.85$; fig. S24, B and C). Changes in enhancer strengths between the two cell types were reflected in the differential mRNA abundance (fig. S25) of the flanking genes (Fig. 4, B and C, and fig. S26): 74% of all enhancers near genes that are fourfold up-regulated in S2 cells appear stronger in S2 cells, whereas only 16% appear stronger in OSCs and vice versa (66% versus 19%). This establishes a direct link between quantitative differences in genome-wide enhancer strengths and differential gene expression. Up to 19% of cell type–specific enhancers were accessible in the cell-type in which they were not active (fig. S27). We also observed 514 genes for which individual enhancers changed more than twofold between cell types, whereas the sum of enhancer activities and the gene expression levels remained constant (<twofold change; fig. S28).

As OSCs have been derived from adult *Drosophila* ovaries and retained marker gene expression and other functional aspects of their in vivo counterparts (*21*), we assessed the activity of 13 OSC STARR-seq enhancers in ovaries of transgenic flies with site-specifically integrated transcriptional reporter constructs. In these flies, 85% (11 out of 13) of the enhancers but none of five control regions were active (Fig. 4D and fig. S29).

Here, we present STARR-seq, which complements ChIP-seq and DHS-seq as the third principal method to study transcriptional regulatory elements in entire genomes. It is unique in its ability to assess enhancer strengths quantitatively and to discover regulatory elements directly based on their ability to enhance transcription, even when silenced endogenously. Applied to two *Drosophila* cell types, it revealed thousands of cell type–specific enhancers with a broad range of strengths and provided the first genome-wide quantitative enhancer activity maps in any organism. STARR-seq is widely applicable to screening arbitrary sources of DNA in any cell type or tissue that allow the efficient introduction of reporter constructs (e.g., by plasmid transfection). This includes human HeLa cells, for which we confirm the quantitative nature of STARR-seq and its ability to identify enhancers that function in luciferase assays independent of their chromatin states and, thus, more reliably than previous methods (figs. S30 and S31). STARR-seq should be widely applied to many cell types across organisms to annotate cell type–specific gene regulatory elements and functionally assess noncoding mutations.

References and Notes

1. J. Banerji, S. Rusconi, W. Schaffner, *Cell* **27**, 299 (1981).
2. M. Levine, *Curr. Biol.* **20**, R754 (2010).
3. J. O. Yáñez-Cuna, E. Z. Kvon, A. Stark, *Trends Genet.* **29**, 11 (2013).
4. N. D. Heintzman *et al.*, *Nature* **459**, 108 (2009).
5. A. P. Boyle *et al.*, *Cell* **132**, 311 (2008).
6. K. J. Gaulton *et al.*, *Nat. Genet.* **42**, 255 (2010).
7. D. S. Johnson, A. Mortazavi, R. M. Myers, B. Wold, *Science* **316**, 1497 (2007).
8. G. Robertson *et al.*, *Nat. Methods* **4**, 651 (2007).
9. A. Melnikov *et al.*, *Nat. Biotechnol.* **30**, 271 (2012).
10. R. P. Patwardhan *et al.*, *Nat. Biotechnol.* **30**, 265 (2012).
11. M. D. Adams *et al.*, *Science* **287**, 2185 (2000).
12. P. V. Kharchenko *et al.*, *Nature* **471**, 480 (2011).
13. modENCODE Consortium *et al.*, *Science* **330**, 1787 (2010).
14. T. J. Parry *et al.*, *Genes Dev.* **24**, 2013 (2010).
15. M. W. Perry, A. N. Boettiger, M. Levine, *Proc. Natl. Acad. Sci. U.S.A.* **108**, 13570 (2011).
16. N. Frankel *et al.*, *Nature* **466**, 490 (2010).
17. L. A. Boyer *et al.*, *Nature* **441**, 349 (2006).
18. A. Rada-Iglesias *et al.*, *Nature* **470**, 279 (2011).
19. M. P. Creyghton *et al.*, *Proc. Natl. Acad. Sci. U.S.A.* **107**, 21931 (2010).
20. S. Bonn *et al.*, *Nat. Genet.* **44**, 148 (2012).
21. K. Saito *et al.*, *Nature* **461**, 1296 (2009).

Acknowledgments: We thank H. K. Akyüz, M. Pagani, K. Schernhuber, D. Spies, H. Tagoh, M. Busslinger, S. Westermann, J. M. Peters, J. Zuber (IMP), J. Brennecke and group, U. Elling [Institute of Molecular Biotechnology (IMBA)], and the IMP/IMBA BioOptics and Graphics Services for help. Deep sequencing was performed at the CSF Next-Generation Sequencing Unit (http://csf.ac.at); Vienna Tile (VT) lines were obtained from the Dickson laboratory via the Vienna *Drosophila* RNAi Center (http://stockcenter.vdrc.at). C.D.A., L.M.B., and M.R. are supported by a European Research Council (ERC) Starting Grant (no. 242922) awarded to A.S. Basic research at the IMP is supported by Boehringer Ingelheim GmbH. C.D.A. and A.S. are authors on a patent application for STARR-seq (EP 12 004 520.8) filed by Boehringer Ingelheim International GmbH. All constructs are available from the authors subject to a Material Transfer Agreement. All deep sequencing data are available at www.starklab.org and GEO (series accession number GSE40739).

Supplementary Materials

www.sciencemag.org/cgi/content/full/science.1232542/DC1
Materials and Methods
Figs. S1 to S31
Tables S1 to S12
References (*22*–*48*)

9 November 2012; accepted 8 January 2013
Published online 17 January 2013;
10.1126/science.1232542

Genomic Analysis of Non-*NF2* Meningiomas Reveals Mutations in *TRAF7*, *KLF4*, *AKT1*, and *SMO*

Victoria E. Clark,[1] E. Zeynep Erson-Omay,[1] Akdes Serin,[1] Jun Yin,[2] Justin Cotney,[2] Koray Özduman,[3] Timuçin Avşar,[4] Jie Li,[5] Phillip B. Murray,[1] Octavian Henegariu,[1] Saliha Yilmaz,[1] Jennifer Moliterno Günel,[6] Geneive Carrión-Grant,[1] Baran Yılmaz,[7] Conor Grady,[1] Bahattin Tanrıkulu,[7] Mehmet Bakırcıoğlu,[1] Hande Kaymakçalan,[8] Ahmet Okay Caglayan,[1] Leman Sencar,[1] Emre Ceyhun,[1] A. Fatih Atik,[7] Yaşar Bayri,[7] Hanwen Bai,[1] Luis E. Kolb,[1] Ryan M. Hebert,[1] S. Bulent Omay,[1] Ketu Mishra-Gorur,[1] Murim Choi,[2] John D. Overton,[9] Eric C. Holland,[10] Shrikant Mane,[2,9] Matthew W. State,[11] Kaya Bilgüvar,[1] Joachim M. Baehring,[12] Philip H. Gutin,[6] Joseph M. Piepmeier,[13] Alexander Vortmeyer,[5] Cameron W. Brennan,[14] M. Necmettin Pamir,[3] Türker Kılıç,[15] Richard P. Lifton,[2,16] James P. Noonan,[2,17] Katsuhito Yasuno,[1] Murat Günel[1,18]*

We report genomic analysis of 300 meningiomas, the most common primary brain tumors, leading to the discovery of mutations in *TRAF7*, a proapoptotic E3 ubiquitin ligase, in nearly one-fourth of all meningiomas. Mutations in *TRAF7* commonly occurred with a recurrent mutation (K409Q) in *KLF4*, a transcription factor known for its role in inducing pluripotency, or with $AKT1^{E17K}$, a mutation known to activate the PI3K pathway. *SMO* mutations, which activate Hedgehog signaling, were identified in ~5% of non-*NF2* mutant meningiomas. These non-*NF2* meningiomas were clinically distinctive—nearly always benign, with chromosomal stability, and originating from the medial skull base. In contrast, meningiomas with mutant *NF2* and/or chromosome 22 loss were more likely to be atypical, showing genomic instability, and localizing to the cerebral and cerebellar hemispheres. Collectively, these findings identify distinct meningioma subtypes, suggesting avenues for targeted therapeutics.

Meningiomas, arising from the meninges of the central nervous system, are the most common primary brain tumors, with a prevalence of ~170,000 cases in the United States (*1*). Although most are histologically classified as benign (grade I), about 10% represent

atypical (grade II) or anaplastic (grade III) forms. Meningiomas frequently invade surrounding brain and critical neurovascular structures, often causing neurological deficits and requiring surgical intervention. Loss of *Neurofibromin 2* (*merlin, NF2*) is found in 40 to 60% of sporadic meningiomas (*2*), but the genetic architecture of the remainder remains obscure, limiting options for the development of rational therapies.

To comprehensively characterize the genomics of meningioma and to gain further insight into molecular mechanisms of tumor formation, we performed genome-wide genotyping and exome sequencing (average depth of coverage 255-fold) of 50 previously nonirradiated grade I (n = 39) and grade II (n = 11) meningiomas and matched normal DNA (*3*) (table S1). For the meningiomas in which matching blood samples were available (n = 39), the mean number of protein-altering somatic mutations was 7.2 (range 1 to 15), a considerably smaller number compared with malignant tumors (table S2). We next searched for genes with significantly more somatic mutations than expected by chance (fig. S1). Besides *NF2*, we identified increased mutation burden in *TNF receptor-associated factor* 7 (*TRAF7*), *Krupple-like factor 4* (*KLF4*), *v-akt murine thymoma viral oncogene homolog 1* (*AKT1*), and *Smoothened, frizzled family receptor* (*SMO*) (as a group, referred to as *non-NF2* mutant hereafter) (Fig. 1). Mutations in these genes were mutually exclusive of *NF2* mutations. In addition, we identified single mutations in genes previously reported to play a role in other neoplasias, including *CREBBP*, *PIK3CA* (R108H variant), *PIK3R1* (deletion p.306-307), and *BRCA1* as well as two *SMARCB1* mutations, which coexisted with *NF2* loss and have previously been reported in meningiomas (*4*) (table S3).

We next performed targeted resequencing of these top five genes, along with chromosome 22 copy-number analysis, in an independent set of 250 unradiated meningiomas (204 grade I and 46 high-grade meningiomas) (fig. S2). In the combined analysis of 300 meningiomas, we identified coding mutations in one of these five genes and/or evidence for chromosome 22 loss in 237 (79%) (Fig. 2A and table S3). *NF2* mutations were present in 108 (36%). *TRAF7* mutations, which were always exclusive of *NF2* mutations [mutual exclusivity P value (P_{me}) = 2.55×10^{-17} (*5*)], were observed in nearly one-fourth of the meningiomas examined (n = 72). TRAF7 is a proapoptotic N-terminal RING and zinc finger domain protein with E3 ubiquitin ligase activity that contains seven WD40 repeats in its C terminus (*6*). TRAF7 interacts with several molecules, such as MEKK3, through these WD40 repeats, affects multiple signaling pathways, including NF-κB, and targets ubiquitination of proteins including c-FLIP, an antiapoptotic molecule (*7*). It is notable that 67 of the 72 TRAF7 mutations, including 15 recurrent mutations, all map to the WD40 domains (Fig. 2B).

In the transcription factor *KLF4*, we identified a recurrent K409Q mutation, which almost always co-occurred with *TRAF7* mutations [n = 31; co-occurrence P value (P_{co}) = 2.50×10^{-20}] and were exclusive of *NF2* mutations (P_{me} = 3.77×10^{-7}). KLF4 is expressed in meningiomas (fig. S3). KLF4 regulates differentiation of several cell types and is best known as one of four genes that together promote reprogramming of differentiated somatic cells into pluripotent stem cells (*8*). Deletion of the KLF4 DNA binding

Tumor	Grade	Chr22 loss	NF2	TRAF7	AKT1	KLF4	SMO
MN-95	1	Yes					
MN-290	1	Yes					
MN-1041	1	Yes					
MN-1047	1	Yes					
MN-1137	1	Yes					
MN-47	1	Yes	p.Q453X				
MN-52	1	Yes	p.F256fs				
MN-71	1	Yes	p.T59fs				
MN-81	1	Yes	p.Q65fs				
MN-169	1	Yes	p.E460X				
MN-288	1	Yes	p.K17_M29del				
MN-291	1	Yes	p.I210fs				
MN-293	1	Yes	p.Q459X				
MN-294	1	Yes	c.363+1G>C				
MN-297	1	Yes	p.K99fs				
MN-301	1	Yes	p.W41fs				
MN-306	1	Yes	p.K44X				
MN-1091	1	Yes	p.L14fs				
MN-1133	1	Yes	p.Y207fs				
MN-26	1			p.C388Y	p.E17K		
MN-105	1			p.R641C	p.E17K		
MN-292	1			p.Q637H	p.E17K		
MN-191	1			p.K615E		p.K409Q	
MN-201	1			p.L580del		p.K409Q	
MN-249	1			p.R641C		p.K409Q	
MN-1025	1			p.G536S		p.K409Q	
MN-1066	1			p.N520S		p.K409Q	
MN-303	1			p.S561N			
MN-206	1			p.G390E			
MN-304	1			p.R653Q			
MN-305	1			p.G536S			
MN-1053	1			p.E353insFRRDAS			
MN-1045	1						p.L412F
MN-1132	1						p.W535L
MN-164	2	Yes					
MN-22	2	Yes	c.115-1G>A				
MN-54	2	Yes	p.Q319X				
MN-96	2	Yes	p.L14fs				
MN-97	2	Yes	p.M426fs				
MN-171	2	Yes	p.L208P				
MN-295	2	Yes	p.E103fs				
MN-298	2	Yes	p.V24fs				
MN-1054	2	Yes	p.R262X				
MN-16	2	Yes		p.T145M	p.E17K		
MN-1144	2	Yes		p.F337S			

Fig. 1. Exome sequencing identifies meningioma subgroups based on mutually exclusive mutation profiles.

[1]Departments of Neurosurgery and Genetics, Yale Program in Brain Tumor Research, Yale School of Medicine, New Haven, CT 06510, USA. [2]Department of Genetics, Yale School of Medicine, New Haven, CT 06510, USA. [3]Department of Neurosurgery, Acibadem University School of Medicine, Istanbul 34848, Turkey. [4]Dr. Orhan Öcalgiray Molecular Biology-Biotechnology and Genetics Research Center, Istanbul Technical University, Maslak 34469, Istanbul, Turkey. [5]Department of Pathology, Yale School of Medicine, New Haven, CT 06510, USA. [6]Department of Neurosurgery and Brain Tumor Center, Memorial Sloan-Kettering Cancer Center, New York, NY 10065, USA. [7]Department of Neurosurgery, Marmara University School of Medicine, Istanbul 34854, Turkey. [8]Department of Genetics and Bioinformatics, Bahcesehir University, Istanbul 34353, Turkey. [9]Center for Genome Analysis, Yale School of Medicine, West Haven, CT 06516, USA. [10]Departments of Cancer Biology and Genetics, Neurosurgery, Neurology, and Surgery, Brain Tumor Center, Memorial Sloan-Kettering Cancer Center, New York, NY 10065, USA. [11]Departments of Genetics and Psychiatry, Yale Program on Neurogenetics and Child Study Center, Yale School of Medicine, New Haven, CT 06510, USA. [12]Departments of Neurology, Neurosurgery, and Internal Medicine, Yale Program in Brain Tumor Research and Yale Brain Tumor Center, Yale School of Medicine, New Haven, CT 06510, USA. [13]Department of Neurosurgery, Yale Program in Brain Tumor Research and Yale Brain Tumor Center, Yale School of Medicine, New Haven, CT 06510, USA. [14]Department of Neurosurgery and Brain Tumor Center, Human Oncology and Pathogenesis Program, Memorial Sloan-Kettering Cancer Center, New York, NY 10065, USA. [15]Department of Neurosurgery, Bahcesehir University School of Medicine, Istanbul 34349 Turkey. [16]Department of Internal Medicine, Howard Hughes Medical Institute, Yale School of Medicine, New Haven, CT 06510, USA. [17]Kavli Institute for Neuroscience, Yale School of Medicine, New Haven, CT 06520, USA. [18]Yale Program on Neurogenetics, Yale School of Medicine, New Haven, CT 06510, USA.

*To whom correspondence should be addressed. E-mail: murat.gunel@yale.edu

domain blocks differentiation and induces self-renewal in hematopoietic cells (*9*). The recurrently mutated KLF4 residue, K409, lies within the first zinc finger and makes direct DNA contact in the major groove of the DNA binding motif (*9*) (Fig. 2C and fig. S4).

The known neoplasia-related recurrent mutation, $AKT1^{E17K}$, was identified in 38 meningiomas. Although the $AKT1^{E17K}$ mutation co-occurred with *TRAF7* mutations in 25 of the 38 tumors ($P_{co} = 3.90 \times 10^{-9}$), it was exclusive of the $KLF4^{K409Q}$ ($P_{me} = 1.18 \times 10^{-2}$) and *NF2* mutations, except in one case ($P_{me} = 2.70 \times 10^{-7}$). The $AKT1^{E17K}$ mutation has been shown to activate PI3K/AKT signaling (*10*) and was readily detectable by immunohistochemistry using an antibody specific for this mutation (fig. S3).

Finally, in 11 tumors, we identified mutations in *SMO*, which is expressed in meningiomas (fig. S5). These mutations include a recurrent L412F variant in seven meningiomas and a previously reported W535L mutation, which has been shown to result in activation of Hedgehog signaling in basal cell carcinoma (*11*). Eight of these SMO mutations were mutually exclusive of mutations in the other four genes ($P_{me} = 1.24 \times 10^{-2}$).

We next evaluated chromosomal instability. Chromosome 22 loss, observed in 149 tumors, was the most common event and was strongly associated with the presence of coding *NF2* mutations ($P_{co} = 1.32 \times 10^{-47}$). These were also significantly associated with higher grade meningiomas [$P = 5.90 \times 10^{-5}$; odds ratio (OR) = 3.54]. Higher-grade tumors also showed an increased number of large-scale chromosomal abnormalities (Fig. 2D and fig. S6) (6.9 versus 1.7 events per tumor) and an increased rate of *NF2* mutations ($P = 0.03$; OR = 1.96) and were observed more frequently in males than females ($P = 6.45 \times 10^{-4}$; OR = 2.93).

Given these observations pointing to distinct tumor subtypes based on mutation profiles, we

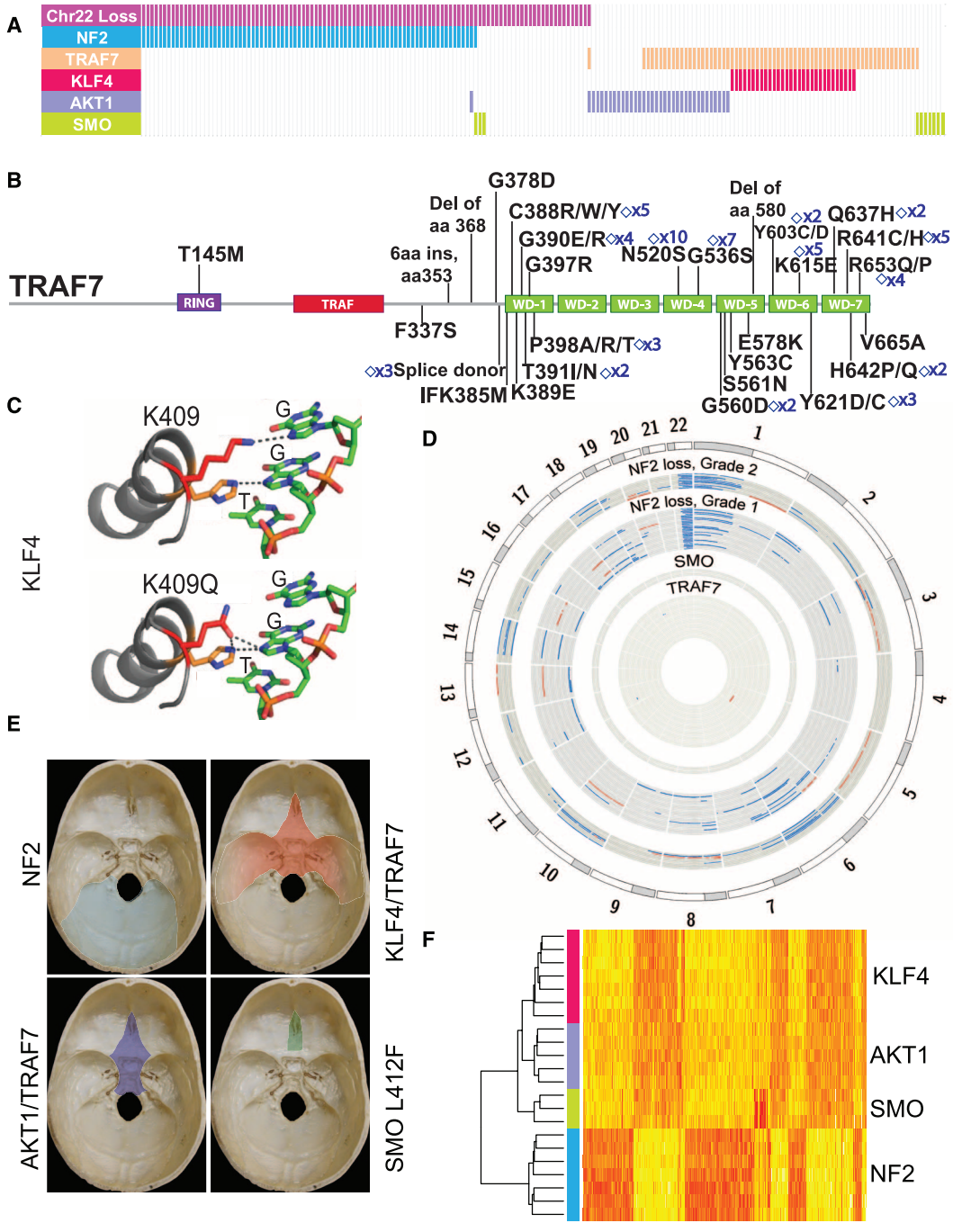

Fig. 2. Genomic architecture of meningiomas. (**A**) *NF2*, *TRAF7*, and *SMO* coding mutations along with recurrent $AKT1^{E17K}$ and $KLF4^{K409Q}$ variants reveal meningioma subtypes with mutually exclusive profiles. Analysis for chromosome 22 copy number is also shown. Each bar represents a grade I meningioma sample; 191 samples are depicted. (**B**) *TRAF7* mutations, which are identified in 72 of 300 meningiomas analyzed, are clustered within its WD40 domains. The count of recurrent mutations, which are denoted by diamonds, is indicated. (**C**) The recurrent $KLF4^{K409Q}$ mutation is located within the first zinc finger domain, which makes direct DNA contact. (**D**) Circos plot of large-scale genomic abnormalities identified (blue: deletion, red: amplification). Whereas all *NF2/chr22loss* meningiomas (outer circles, $n = 41$, including $n = 30$ with coding *NF2* mutations) show chromosome 22 loss, which is typically associated with further chromosomal abnormalities in grade II tumors ($n = 11$, including $n = 8$ with coding *NF2* mutations), genomic stability is a hallmark of grade I *non-NF2* tumors (inner circles, $n = 36$). (**E**) Along the skull base, *NF2/chr22loss* meningiomas originate from the lateral and posterior regions, whereas the vast majority of anterior and medial meningiomas are *non-NF2* mutant. (**F**) Unsupervised hierarchical clustering of gene expression profiles defines two major benign meningioma subgroups, those with *NF2/chr22loss* and *non-NF2* mutant tumors. Each subgroup reveals differential H3K27ac and gene expression profiles (figs. S10 to S14 and tables S5 to S8).

examined whether the mutation spectrum correlated with anatomical distribution and histological subtype. We initially grouped cerebral meningiomas into those originating along the skull base or those present in the cerebral hemispheres (Fig. 2E, fig. S7, and table S4). Interestingly, tumors with *NF2* mutations and/or chromosome 22 loss (*NF2/chr22loss*) were predominantly found in the hemispheres ($P = 9.22 \times 10^{-14}$; OR = 6.74) with nearly all posterior cerebral (parieto-occipital), cerebellar, or spinal meningiomas being *NF2/chr22loss* tumors (fig. S8). For the meningiomas originating from the skull base, we observed a difference between those originating from medial versus lateral regions. The vast majority of *non-NF2* meningiomas were medial ($P = 4.36 \times 10^{-8}$; medial versus lateral OR = 8.80), whereas the lateral and posterior skull base meningiomas had *NF2/chr22loss* ($P = 1.55 \times 10^{-12}$; OR = 23.11). Meningiomas with only the recurrent *SMO* L412F mutation ($n = 5$) all localized to the medial anterior skull base, near the midline. This is particularly interesting because mutations in Hedgehog signaling result in holoprosencephaly, the midline failure of embryonic forebrain to divide into two hemispheres (*12*).

Mutational profiles also were correlated with histological diagnoses. For example, all of the meningiomas with a "secretory" component ($n = 12$), which follow a more aggressive clinical course owing to increased brain swelling, carried both *TRAF7* and *KLF4* mutations ($P_{co} = 6.02 \times 10^{-12}$) (fig. S9).

Consistent with these clinical observations, unsupervised hierarchical clustering of meningiomas based on gene expression and chromatin immunoprecipitation for H3K27 acetylation followed by sequencing (H3K27ac ChIP-seq) analyses confirmed clustering into *NF2/chr22loss* versus *non-NF2* mutant subgroups (Fig. 2F and figs. S10 and S11) and revealed several molecules whose acetylation and expression was specific to a subtype (tables S5 and S6). For these differentially expressed genes, there was a strong correlation between expression and ChIP-seq data (fig. S12). Among the *non-NF2* meningiomas, *SMO* mutants were clearly defined by increased expression and activation of the Hedgehog pathway (fig. S13 and tables S7 and S8).

These results clearly identify meningioma subgroups, distinguishing them based on their mutually exclusive distribution of mutations, distinct potential for chromosomal instability and malignancy, anatomical location, histological appearance, gene expression, and H3K27ac profile. Our results show that the mutational profile of a meningioma can largely be predicted based on its anatomical position, which in turn may predict likely drug response (e.g., Hedgehog inhibitors for midline tumors). This may prove relevant for surgically unresectable, recurrent, or invasive meningiomas and could spare patients surgery or irradiation, an independent risk factor for progression of these generally benign tumors.

References and Notes

1. J. Wiemels, M. Wrensch, E. B. Claus, *J. Neurooncol.* **99**, 307 (2010).
2. M. J. Riemenschneider, A. Perry, G. Reifenberger, *Lancet Neurol.* **5**, 1045 (2006).
3. Materials and methods are available as supplementary materials on *Science* Online.
4. U. Schmitz *et al.*, *Br. J. Cancer* **84**, 199 (2001).
5. Q. Cui, *PLoS ONE* **5**, e13180 (2010).
6. L. G. Xu, L. Y. Li, H. B. Shu, *J. Biol. Chem.* **279**, 17278 (2004).
7. T. Bouwmeester *et al.*, *Nat. Cell Biol.* **6**, 97 (2004).
8. K. Takahashi *et al.*, *Cell* **131**, 861 (2007).
9. A. Schuetz *et al.*, *Cell. Mol. Life Sci.* **68**, 3121 (2011).
10. J. D. Carpten *et al.*, *Nature* **448**, 439 (2007).
11. J. Xie *et al.*, *Nature* **391**, 90 (1998).
12. E. Roessler *et al.*, *Nat. Genet.* **14**, 357 (1996).

Acknowledgments: We are grateful to the patients and their families who have contributed to this study. This study was supported by the Gregory M. Kiez and Mehmet Kutman Foundation. R.P.L. is an investigator of the Howard Hughes Institute. V.E.C. is supported by NIH T32GM07205. All somatic mutations identified through exome sequencing of meningiomas are reported in the supplementary materials and submitted to the Catalogue of Somatic Mutations in Cancer (COSMIC) database (http://cancer.sanger.ac.uk/cancergenome/projects/cosmic, submission ID COSP30702). Yale University has filed a provisional patent application based on the results of this study.

Supplementary Materials

www.sciencemag.org/cgi/content/full/science.1233009/DC1
Materials and Methods
Figs. S1 to S14
Tables S1 to S8
References (*13*–*27*)

24 May 2012; accepted 15 January 2013
Published online 24 January 2013;
10.1126/science.1233009

Unraveling the Mechanism of Protein Disaggregation Through a ClpB-DnaK Interaction

Rina Rosenzweig,[1,2,3]* Shoeib Moradi,[1] Arash Zarrine-Afsar,[2] John R. Glover,[1] Lewis E. Kay[1,2,3,4]*

HSP-100 protein machines, such as ClpB, play an essential role in reactivating protein aggregates that can otherwise be lethal to cells. Although the players involved are known, including the DnaK/DnaJ/GrpE chaperone system in bacteria, details of the molecular interactions are not well understood. Using methyl–transverse relaxation–optimized nuclear magnetic resonance spectroscopy, we present an atomic-resolution model for the ClpB-DnaK complex, which we verified by mutagenesis and functional assays. ClpB and GrpE compete for binding to the DnaK nucleotide binding domain, with GrpE binding inhibiting disaggregation. DnaK, in turn, plays a dual role in both disaggregation and subsequent refolding of polypeptide chains as they emerge from the aggregate. On the basis of a combined structural-biochemical analysis, we propose a model for the mechanism of protein aggregate reactivation by ClpB.

The 580-kD hexameric ClpB molecular chaperone is a bacterial adenosine 5′-triphosphate (ATP)–dependent protein-remodeling machine that rescues stress-damaged proteins trapped in an aggregated state and plays a key role in thermotolerance development and in cell recovery after acute stress (*1*–*3*). Aggregate reactivation requires the collaboration of a second ATP-dependent molecular chaperone system, Hsp70/DnaK (*1*, *4*–*7*). DnaK binding to client proteins is, in turn, regulated by co-chaperones DnaJ and GrpE through modulation of the DnaK ATPase cycle (*8*). A molecular picture of the ClpB-DnaK complex is critical to elucidate the mechanism of protein disaggregation, yet this system has proven recalcitrant to detailed structural studies.

Nuclear magnetic resonance (NMR) spectroscopy is especially suited to characterize protein complexes at atomic detail, even if the interactions are weak and transient. Methyl–transverse relaxation–optimized spectroscopy (TROSY)–based experiments (*9*) and labeling schemes, whereby Ile, Leu, and Val methyl groups are $^{13}CH_3$-labeled in an otherwise highly deuterated background (referred to as ILV-protein) (*10*), have enabled NMR studies of large molecular systems (*11*, *12*), such as those involved in disaggregation. Using these methods, we set out to elucidate the DnaK binding site on the ClpB chaperone.

Because of the large size of each monomer of ClpB (97 kD), NMR spectra of the ILV-labeled protein overlapped, precluding detailed analyses of the full-length molecule (fig. S1). We separately analyzed two monomeric fragments, including (i) $ClpB^{\Delta NBD2}$, comprising the N-terminal domain (NTD), nucleotide binding domain 1 (NBD1), and the coil-coil domain (CCD), and (ii) nucleotide

[1]Department of Biochemistry, University of Toronto, Toronto, Ontario M5S 1A8, Canada. [2]Department of Chemistry, University of Toronto, Toronto, Ontario M5S 3H6, Canada. [3]Department of Molecular Genetics, University of Toronto, Toronto, Ontario M5S 1A8, Canada. [4]Program in Molecular Structure and Function, Hospital for Sick Children, Toronto, Ontario M5G 1X8, Canada.

*To whom correspondence should be addressed. E-mail: rina.rosenzweig@utoronto.ca (R.R.); kay@pound.med.utoronto.ca (L.E.K.)